Investigation of ^{50}Cr(d,n)^{51}Mn and ^{nat}Cr(p,x)^{51}Mn processes with respect to the production of the positron emitter ^{51}Mn

By A. T. J. Klein[†], F. Rösch[††] and S. M. Qaim[*]

Institut für Nuklearchemie, Forschungszentrum Jülich GmbH, D-52425 Jülich, Germany

Summary. The positron emitter ^{51}Mn ($t_{1/2} = 46.2$ min, $I_{\beta^+} = 97\%$) is of potential interest in positron emission tomography (PET). With a view to optimizing its production route, excitation functions for deuteron induced nuclear reactions on isotopically enriched ($\sim 95\%$) ^{50}Cr were determined radiochemically over the energy range of 3 to 13 MeV and for proton induced nuclear reactions on ^{nat}Cr in the range of 18 to 38 MeV. Cross sections are presented for the reactions: ^{50}Cr(d,2n)^{50m}Mn, ^{50}Cr(d,n)^{51}Mn, ^{50}Cr(d,t)^{49}Cr, ^{50}Cr(d,p)^{51}Cr, ^{50}Cr(d,α)^{48}V, ^{52}Cr(d,2p)^{52}V, ^{nat}Cr(p,x)^{51}Mn, ^{nat}Cr(p,x)^{52}Mn, ^{nat}Cr(p,x)^{52m}Mn, ^{nat}Cr(p,x)^{54}Mn, ^{nat}Cr(p,x)^{48}Cr, ^{nat}Cr(p,x)^{49}Cr, ^{nat}Cr(p,x)^{51}Cr, ^{nat}Cr(p,x)^{48}V and ^{nat}Cr(p,x)^{45}Ti. In the case of proton induced reactions on ^{nat}Cr, the isomeric cross section ratio for the isomeric pair ^{52m,g}Mn was also determined. The results are interpreted in terms of the spins of the two isomers concerned. Theoretical thick target yields were derived from the corresponding excitation functions. The maximum achievable thick target yield of ^{51}Mn is 1.1 GBq/μAh in the case of the ^{50}Cr(d,n)^{51}Mn reaction at $E_d = 14 \rightarrow 3$ MeV, and 3.2 GBq/μAh in the case of the ^{nat}Cr(p,x)^{51}Mn process for $E_p = 40 \rightarrow 20$ MeV. The ^{50}Cr(d,n)^{51}Mn process is the favourable production route for ^{51}Mn, since the radioisotopic purity is high and a small-sized medical cyclotron is adequate to produce this positron emitter in sufficient quantities.

Introduction

^{51}Mn is an almost pure positron emitter ($I_{\beta^+} = 97\%$, $E_{\beta^+ \text{(max)}} = 0.935$ MeV, $E_\gamma = 749.1$ KeV, $I_\gamma = 0.265\%$ [1]) with a half-life of 46.2 min, and is thus a principal candidate for positron emission tomography (PET). A particular aim of developing ^{51}Mn labelled radiopharmaceuticals might be the bridging of PET and MRI (magnetic resonance imaging). A class of MRI contrast agents (magnetopharmaceuticals) based on manganese as paramagnetic contrast enhancer is currently being studied. Since biodistribu-

tion and uptake kinetics of magnetopharmaceuticals are hardly quantifiable by means of MRI in man, analogous ^{51}Mn labelled contrast agents might be analyzed instead, using PET. Thus, an evaluation of magnetopharmaceuticals by means of quantitative PET would be enabled.

Potential reactions to produce ^{51}Mn on a MBq scale are listed in Table 1, together with their energy thresholds (calculated from nuclide masses given in ref. [2]), estimated Coulomb barriers, advantages and disadvantages. The two most promising nuclear reactions are ^{50}Cr(d,n)^{51}Mn and ^{52}Cr(p,2n)^{51}Mn. The first reaction has already been applied to produce ^{51}Mn using ^{50}Cr$_2$O$_3$ as target [3− 8]. However, the cross section data are not well known. The excitation function was first determined by Cogneau *et al.* [9] using natural chromium as target and a GM counter for activity measurement. For the ^{nat}Cr(p,x)^{51}Mn process, on the other hand, no cross section data were available up to now. For a comparison of the two processes, a determination of the excitation functions was mandatory. Furthermore, two chemical aspects needed to be addressed in order to quantify ^{51}Mn, namely preparation of thin targets via electroplating of isotopically enriched ^{50}Cr on gold backings, and development of a rapid procedure for the radiochemical separation of ^{51}Mn from irradiated chromium targets. Both these aspects were amply treated in this work while measuring cross sections relevant to the production of ^{51}Mn.

Materials and methods

Target materials

Isotopically enriched ^{50}Cr (94.7%) was used as target material as purchased in metallic form from EURISO-TOP, Groupe CEA, Saint-Aubin Cedex, France and from CHEMOTRADE, Leipzig, Germany. The isotopic composition, confirmed by ICP-MS measurements at the ZCH, Forschungszentrum Jülich, Germany, was: ^{50}Cr (94.7 ± 0.4%), ^{52}Cr (4.84%), ^{53}Cr (0.37%), ^{54}Cr (0.09%). The chemical impurities, as specified by the supplier were: Ti (<30 ppm), Mn (<10 ppm), Fe (<250 ppm), Ni (<40 ppm), Cu (80 ppm), Al (780 ppm), Si (200 ppm) and Ca (150 ppm).

Chemicals

Ion-exchange resins DOWEX 50WX8 and DOWEX 1X8 in different mesh sizes were obtained in specially cleaned

───────────
† Present address: Abteilung Nuklearmedizin, Universitätsklinikum Ulm, D-89081 Ulm, Germany
†† Present address: Institut für Kernchemie, Johannes Gutenberg-Universität, D-55099 Mainz, Germany
* Author for correspondence
(E-mail: S.M.QAIM@FZ-JUELICH.DE).

Table 1. Survey of potential nuclear reactions for ^{51}Mn production.

Nuclear reaction	Energy threshold[a] [MeV]	Coulomb barrier[b] [MeV]	Expected radioisotopic contamination	Advantages	Disadvantages
^{50}Cr(d,n)^{51}Mn	0.00	5.3	none	small cyclotron sufficient ^{nat}Cr as target	enriched target mandatory
^{52}Cr(p,2n)^{51}Mn	16.34	6.6	^{52m,g}Mn		
^{50}Cr(^{3}He,2n)^{51}Fe → ^{51}Mn	11.93	9.3	^{52m,g}Mn		enriched target mandatory
^{50}Cr(^{3}He,pn)^{51}Mn	2.60	9.3			
^{54}Fe(p,α)^{51}Mn	3.21	7.1	^{52m,g}Mn	small cyclotron sufficient ^{nat}V as target	enriched target mandatory
^{51}V(^{3}He,3n)^{51}Mn	14.03	8.8	^{52m,g}Mn		

a: Calculated using nuclide masses [2].
b: Calculated by an approximate classical formula, considering only Coulomb barrier for compound nucleus formation [2].

grade from FLUKA, Buchs, Switzerland. Inorganic reagents such as CrO_3, $CrCl_3$, NaOAc, quartz and oxalic acid were from MERCK, Darmstadt, Germany and solvents like CH_3CN, EtOH and acetone, as well as aqueous acids and bases like HCl, H_2SO_4 or NH_3 from Riedel-de Haën, Frankfurt, Germany.

Instruments

Gravimetric weighing was done using the digital weight AT 261 Delta-Range from METTLER-TOLEDO. Exact pH measurements were carried out with the pH meter CG 838 and the glass electrode type N5900A from SCHOTT, Mainz, Germany. Colorimetric determination of concentrations was performed by the UV/VIS spectrophotometer UV 160A from SHIMADZU, Japan. Quantitative γ-ray spectrometry was conducted using Ge(Li) and HPGe detectors from CANBERRA, Meriden, CT, USA and PERKIN ELMER/ORTEC, Oak Ridge, TN, USA.

Software used for radioactivity analysis

The GammaVision_2.3 PC software from PERKIN ELMER/ORTEC was used for γ-spectrometric data acquisition, graphical presentation and peak area analysis. A databank of γ-lines, including their respective branching ratios, helped to assign the nuclides to the observed photopeaks. Each peak integration was done manually, i.e. the automatic integration mode was not activated. The peak area given by the software includes a statistical error, which considers mainly the Poisson standard deviation $\sigma = \pm \sqrt{\text{peak area}}$.

Multidecay analysis of complex decay curves was performed using the ORIGIN_3.5 software from MICROCAL Software Inc., Northampton, MA, USA. The curve fitting option of the PC program allowed a least squares fit iteration for free parameters of any self-defined mathematical formula. The fitting algorithm also enabled a weighted fitting of the experimental data points, e.g. depending on their ordinate errors.

Target preparation

Targets were prepared by electrodeposition of metallic ^{50}Cr° on gold cathodes, serving as chemically inert backings during and after the irradiation. Metallic filings of ^{50}Cr° converted almost quantitatively to pure ^{50}CrO$_3$. The electrolyte was obtained by dissolution of the trioxide

Table 2. Applied electrodeposition parameters for thin ^{50}Cr° target preparation.

$c(^{50}CrO_3) \cdot$ aq [M]	0.13	Anode	Pt
$c(H_2SO_4)$ [M]	0.01	Anode plane [cm²]	0.6
$V_{Electrolyte}$ [mL]	1.5	Cathode	Au
T [°C]	21	Cathode plane [cm²]	1.076
t [min]	10		
I′ [mA cm^{-2}]	140		

in dilute H_2SO_4. A compact electrolysis cell, developed in our institute [10−12] was used. Layers of about 1.7 mg cm^{-2} (2.4 μm) thickness were produced using the deposition parameters listed in Table 2 (for more details cf. [12]). The chromium depositions were washed with water and acetone and finally air dried. The deposition yield was estimated initially by weighing. After the irradiation, followed by chemical separation and γ-ray spectrometry, the chromium content of the sample was determined exactly by colorimetric, i.e. by spectrophotometric determination of chromate in the Cr-fraction (cf. [12]). The amount of chromium obtained by this method was used to calculate the plane weight and the thickness of the ^{50}Cr° target layer. In addition, the electrolytes used were occasionally checked for the isotopic content by ICP-MS analysis. It could be verified, that no isotope dilution by chromium of natural composition occurred during the chemical preparation and recovery process. However, a high Si content in the range of 30 mole-% relative to Cr was simultaneously observed; it was due to the preparative process.

Cyclotron irradiations

All deuteron irradiations up to 13.5 MeV and some proton irradiations up to 22 MeV were performed at the compact cyclotron CV 28 of the Forschungszentrum Jülich GmbH. The nominal beam current was 300 nA for deuterons and < 200 nA in proton experiments, measured by means of a Faraday cup. Proton irradiations were done mostly at the Injector of COSY, with proton energies up to 45 MeV. In this facility sample foils were irradiated inside the cyclotron vacuum using a specially designed target holder [13].

In all experiments the well established stacked-foil technique was applied (cf. [14−16]). Each stack consisted of two target foils in irradiations at the CV 28 and of nine in a single experiment at the Injector cyclotron. Each stack contained also at least two monitor foils. The energy effec-

tive at each foil inside the stack was determined using the iterative EXCEL program STOP_POW.xls, which was optimised in our institute. It was based on the equations of charged particle energy loss in matter (cf. [17]).

Monitor reactions

In the case of deuteron bombardments, excitation functions of the nuclear reactions ^{54}Fe(d,n)^{55}Co [18], ^{52}Cr(d,2n)^{52}Mn [19], ^{197}Au(d,2n)^{197m}Hg [20] and ^{nat}Ti(d,x)^{48}V [21] were applied as monitor reactions. After our experiments new data became available for the reactions ^{54}Fe(d,n)^{55}Co [22] and ^{nat}Ti(d,x)^{48}V [23]; however, we did not consider them. The errors for the graphically given cross section data were self-estimated according to the quality of determination of the respective monitor reaction. The chosen relative errors are 6, 7, 8 and 12% for the above mentioned monitor reactions, respectively. In proton irradiations, the monitor reactions ^{nat}Cu(p,x)^{62}Zn [24, 25], ^{nat}Cu(p,x)^{63}Zn [25, 26], ^{27}Al(p,3pn)^{24}Na [27], ^{27}Al(p,αpn)^{22}Na [28] and ^{nat}Cr(p,x)^{52}Mn [19] were used (cf. [29]). In all those cases, errors for the cross sections are given in the literature.

The derived weighted mean particle fluxes inside the stack were obtained from individually determined fluxes in the monitor foils using the cross section errors as weighting tool.

Projectile energies

At the CV 28 the primary deuteron energy was measured by a TOF method [30] as 13.4 ± 0.2 MeV. Protons of about 22 MeV were available only with low fluxes and their exact energy could not be determined on-line. In those cases the copper monitor foils with their different well known nuclear reactions leading to the three zinc nuclides ^{62}Zn, ^{63}Zn and ^{65}Zn were used (cf. [16, 31]). The proton energy at the Injector of COSY was determined as 45.6 ± 0.2 MeV. The desired target energies were obtained using a different number of incident Al absorber foils in front of the relevant stack.

Radiochemical separations

Radiochemical separations were applied to study the ^{50}Cr(d,x) reactions. After an initial non-destructive γ-ray spectrometric measurement of about 5 min, a sequential processing of the two ^{50}Cr°/Au° foils was done (cf. [11, 32, 33]). Each target was treated with 2 mL of a hot 3 M HCl. After about 20 sec the unleached inert gold foil was removed and measured later γ-spectrometrically, since the backing foil was simultaneously used as monitor foil. Then 1 mL of water and 1 mL of a 10 M NaOH were added to the solution. Further addition of about 1 mL of a 10 M H_2O_2 solution in the heat oxidized chromium(III) to chromate, resulting in a color change from green-grey over brown to light yellow after about 30 sec. Next, 1 mL of a 6 mM $FeCl_3$ solution was added dropwise, whilst the peroxide was decomposed catalytically and the Fe^{III} precipitated as hydroxide, coprecipitating with n.c.a. ^{51}MnO$_2$. After a short boiling ($\sim$ 1 min) the solution was given onto a special filter column and was pressed through it by slight

air pressure. The filter column (d_i = 10 mm) consisted of two layers of about 1 cm height each, a lower one of silica gel (60/80 mesh) and an upper one of coarse-grained quartz powder (200−800 μm), which adsorbed already most of the voluminous ferrous hydroxide. The columns were conditioned before use by means of the sequence: 5×2 mL 7 M HCl, 5×2 mL H_2O, and 2×2 mL 0.1 M NaOH. The precipitate was washed 8 times with 1 mL of a warm 0.1 M NaOH. The chromate filtrate was collected and subsequently evaporated. Iron and co-adsorbed radiomanganese were desorbed from the column by means of 8 portions of 1 mL warm 3 M HCl. The collected Fe/Mn-fraction was evaporated simultaneously with the Cr-fraction nearly to dryness.

As separation time $t^\#$ the start of the precipitate washing with dilute NaOH, about 10 min after the beginning of the procedure, was used. The required time for the manual separation process was 17 min. Additional 20 min and 40 min were needed to evaporate the Mn- and the Cr-fraction, respectively. The radiochemical separation efficiencies $(1\text{-}\kappa)$ and $(1\text{-}\tau)$ were determined in advance by tracer experiments, but were also accessible via many irradiated target foils using the indicator nuclides ^{48}V and ^{51}Mn for the distribution of radiochromium and radiomanganese, respectively (cf. below). The factor τ denotes the fraction of total Mn remaining in the Cr-fraction and the factor κ the fraction of total Cr remaining in the Mn-fraction after radiochemical separation at the time $t^\#$ after EOB (t = 0).

Identification of radionuclides and measurement of radioactivity

The radioactive products were identified by their characteristic emitted radiation and by their half-lives. The decay data used are summarized in Table 3. In all cases γ-ray spectrometry was applied. The identification of ^{50m}Mn, ^{52m}Mn, ^{52}Mn, ^{48}Cr, ^{49}Cr, ^{48}V and ^{52}V was relatively straightforward. In the case of ^{54}Mn, ^{51}Cr, ^{51}Mn and ^{45}Ti, however, some special techniques were necessary.

^{54}Mn was detected in proton irradiation experiments using the 834.8 keV γ-ray. Due to the low abundance of the relevant target nuclide ^{54}Cr in ^{nat}Cr and the long half-life of ^{54}Mn (312.2 d), the radionuclide could only be quantified via γ-ray measurements for periods > 20 h using a specially shielded detector with very low background. Peak areas of about 500 counts were obtained.

^{51}Cr was quantified in the radiochemically separated Cr fraction via its 320.1 keV γ-line. It was a cumulative activity, i.e. a sum of the activity formed directly through a nuclear reaction as well as via the decay of ^{51}Mn. Since the absolute ^{51}Mn activity was determined independently, the directly formed ^{51}Cr fractions could be calculated from the cumulative activity, subtracting the indirectly formed contribution.

In deuteron irradiation experiments the calculations became a bit more complex due to the chemical separation, making a knowledge of the exact separation time $t^\#$ and the separation efficiency $(1\text{-}\kappa)$ and $(1\text{-}\tau)$ mandatory. The independently formed ^{51}Cr activity by direct nuclear processes is extracted from the cumulative activity by formula (1). In total, three terms have to be subtracted from the

Nuclide	Half-life	I_{β^+} [%]	I_{IT} [%]	$E_\gamma{}^a$ [keV]	I_γ [%]
^{45}Ti	3.08 h	85	–	719.1	0.154
^{48}V	15.98 d	50	–	983.5	99.99
^{52}V	3.7 min	(β^-)	–	1434.1	100
^{48}Cr	21.56 h	1.47	–	308.3	100
^{49}Cr	42.1 min	93	–	152.9	30.9
^{51}Cr	27.7 d	–	–	320.1	9.8
^{50m}Mn	1.7 min	99	–	783.3	91.3
^{51}Mn	46.2 min	97	–	749.1	0.265
^{52m}Mn	21.1 min	97	1.75	1434.1	98.2
^{52}Mn	5.6 d	29	–	744.2	90
^{54}Mn	312.2 d	–	–	834.8	99.98
^{22}Na^b	950.5 d	89.4	–	1274.5	99.94
^{24}Na^b	14.96 h	–	–	1368.6	100
^{55}Co^b	17.53 h	76	–	477.2	20.2
^{62}Zn^b	9.26 h	8.4	–	596.7	25.7
^{63}Zn^b	38.1 min	93	–	669.8	8.4
^{65}Zn^b	244.1 d	1.46	–	1115.5	50.8
^{197m}Hg^b	23.8 h	–	93	134.0	34.1

Table 3. Decay data of reaction products used in the determination of absolute activity.

a: Used γ-line. b: In monitor foils only.

cumulative activity (term 2 on the right side) considering the fractions from ^{51}Mn decay during the irradiation, between EOB and $t^\#$ and after $t^\#$:

$$A(^{51}\text{Cr})_0 = A(^{51}\text{Cr})^0_{\text{Cr}} \\ - \{A(^{51}\text{Cr})^0_{\text{B}} + A(^{51}\text{Cr})^0_{t^\#} + A(^{51}\text{Cr})^0_{\oplus}\}. \quad (1)$$

The cumulative ^{51}Cr activity — i.e. term 1 on the right side of formula (1) — in the Cr-fraction is described by:

$$A(^{51}\text{Cr})^0_{\text{Cr}} = \left(\frac{1}{1-\kappa}\right) \cdot A(^{51}\text{Cr})_{\text{Cr}}(t) \cdot \tfrac{1}{2}^{\frac{t}{t_{\text{Cr}}}} \quad (2)$$

with the unseparated fraction κ of the total chromium remaining in the Mn-fraction, and with the measured activity $A(^{51}\text{Cr})_{\text{Cr}}(t)$ of ^{51}Cr in the Cr-fraction at the time t. The other terms in (1) are expressed by:

$$A(^{51}\text{Cr})^0_{\text{B}} = A(^{51}\text{Mn})_0 \cdot \left(\frac{t_{\text{Mn}}}{t_{\text{Cr}}}\right)\left(\frac{\lambda_{\text{Mn}}t_{\text{B}}}{(1-e^{-\lambda_{\text{Mn}}t_{\text{B}}})} - 1\right) \cdot \tfrac{1}{2}^{\frac{t_{\text{B}}}{t_{\text{Cr}}}} \quad (3)$$

$$A(^{51}\text{Cr})^0_{t^\#} = A(^{51}\text{Mn})_0 \cdot \left(\frac{t_{\text{Mn}}}{t_{\text{Cr}}}\right) \cdot \left(1 - (\tfrac{1}{2})^{\frac{t^\#}{t_{\text{Mn}}}}\right) \quad (4)$$

$$A(^{51}\text{Cr})^0_{\oplus} = \tau \cdot \left[A(^{51}\text{Mn})_0 \cdot \frac{t_{\text{Mn}}}{t_{\text{Cr}}} \cdot \tfrac{1}{2}^{\frac{t^\#}{t_{\text{Mn}}}}\right] \quad (5)$$

with $A(^{51}\text{Mn})_0$ as the EOB activity of ^{51}Mn, λ_{Mn} the decay constant of ^{51}Mn and t_{B} the irradiation time. t_{Mn} represents the half-life of ^{51}Mn and t_{Cr} that of ^{51}Cr. Formula (3) describes term 2 on the right side of formula (1), taking into account the contribution of ^{51}Cr stemming from the ^{51}Mn decay during the irradiation and formula (4) describes term 3 in (1), considering further ^{51}Cr due to ^{51}Mn decay between EOB and separation time $t^\#$. Beyond this, formula (5), describing term 4 in (1), considers additional ^{51}Cr in the separated Cr-fraction stemming from the fraction τ of total ^{51}Mn, which remained in the Cr-fraction after separation under real conditions.

^{51}Mn activity was determined using two or more of the following four methods.

(I) Non-destructive (ND method) measurement of the annihilation peak. The 511 keV line was completely assigned to the positron emission of ^{51}Mn in a single γ-ray measurement directly after EOB.

(II) Multidecay analysis (MDA method) of the annihilation peak; in deuteron irradiation experiments after radiochemical separation of the radiomanganese fraction. Usually, besides ^{51}Mn only ^{52}Mn was identified in the decay curve at a later cooling time. In cases where no chemical separation was done (deuteron irradiations to study ^{50m}Mn and proton irradiations), activities of ^{51}Mn and ^{45}Ti could be extracted from the complex decay curve using prescriptions for present nuclides with additional discrete γ-lines for nuclides such as ^{52m}Mn, ^{52}Mn, ^{48}Cr, ^{49}Cr and ^{48}V in the fit option of ORIGIN. The error of determination was in the range of 8% for ^{51}Mn but more than 25% for ^{45}Ti.

(III) Quantification of the ^{51}Cr daughter (DAU method) in the separated Mn-fraction.

The ^{51}Mn activity derived from the activity of the daughter ^{51}Cr was given by the formula:

$$A(^{51}\text{Mn})_0 = \\ \left(\frac{1}{1-\tau}\right) \cdot [A(^{51}\text{Cr})^0_{\text{Mn}} - \kappa \cdot A(^{51}\text{Cr})^0_{\text{Cr}}] \cdot \left(\frac{t_{\text{Cr}}}{t_{\text{Mn}}}\right) \cdot 2^{\frac{t^\#}{t_{\text{Mn}}}} \quad (6)$$

where $A(^{51}\text{Mn})_0$ is the desired ^{51}Mn activity at EOB, $A(^{51}\text{Cr})^0_{\text{Mn}}$ the ^{51}Cr activity in the Mn-fraction after complete decay of ^{51}Mn, and $A(^{51}\text{Cr})^0_{\text{Cr}}$ the ^{51}Cr activity in the Cr-fraction, extrapolated to EOB, respectively.

(IV) Counting the 749.1 keV characteristic photopeak (CP method). Due to the very weak intensity of this γ-ray ($I_\gamma = 0.265\%$) and due to its overlap with the 744.2 keV γ-line of ^{52}Mn, the derived activities have a high error.

In deuteron induced reactions, the final mean absolute activity $\bar{A}$ of ^{51}Mn was calculated as a weighted mean of the four determination methods. The weighting w(i) for the

i-method thereby resulted from fixed standard weightings W(i) and the respective activities A(i):

$$\bar{A} = \sum_i A(i) \cdot w(i) = \sum_i \left(A(i) \cdot \frac{W(i)}{\sum_i W(i)} \right). \qquad (7)$$

Fixed standard weightings W(i) = 40, 30, 20 and 10 (%) were chosen for the methods i = ND, MDA, DAU and CP, respectively. We have chosen a relatively high weighting for the ND method, since the other methods all contained a relatively high "chemistry error" resulting from the separation procedures. Seen from another point of view we weighted all determination methods following radiochemical separation with not less than 60 %. The ND method, of course, contained some contributions from other simultaneosly formed positron emitters dominating initially (i.e. about 30 min) after EOB, mainly ^{52m}Mn, ⁴⁹Cr and ⁴⁸V. The first two are present due to their short half-lives, i.e. their high activation during the irradiation. Both nuclides appear at higher deuteron energies > 8 MeV (for thresholds cf. e.g. [33]). ⁴⁸V disturbs at that time (though its half-life is longer) due to the low reaction threshold and relatively high cross section as demonstrated by Fig. 5. The weighting for the CP data was chosen as low, since the characteristic photopeak of ⁵¹Mn occurs only with a low transition probability.

In proton irradiation experiments only two methods of ⁵¹Mn final mean activity determination were accessible, namely the MDA and the CP method, since no separation was done. The weighted mean here was calculated using again formula (7) with the same W(i), i.e. the same weighting ratio as in deuteron experiments, i.e. 30 : 10 for the MDA and CP method, respectively.

An attempt was made to quantify ⁴⁵Ti in proton irradiation experiments by means of its annihilation radiation from the multidecay curve. However, the activity values obtained for this nuclide have errors up to 30 % due to the high activities of ⁵¹Mn and ^{52m}Mn.

Determination of absolute activities

The nuclide specific γ-rays and their intensities were taken from [1] and are summarized in Table 3. The detector efficiencies were determined using standards with absolute activities known within $\pm$ 3 %.

Dead time correction was automatically performed by the multichannel analyzer during the measurement. The count rates were converted to absolute activities using the standard conversion formula:

$$A(t^*) = \frac{I/M}{I_\gamma \, \varepsilon_D(\delta,E) \, GF}. \qquad (8)$$

I is the number of counts, M the effective measuring time (life time), t* the time of the measurement, $\varepsilon_D(\delta,E)$ the detector efficiency and GF the geometric factor (GF $\leq$ 1) of the sample.

As time of the measurement t*, the expression t* = t + α t$_R$ was used, with the starting time t, the measuring time t$_R$ (real time) and the time enhance factor α. The factor was

given by:

$$\alpha = \frac{\ln\left(\dfrac{\lambda M}{1 - e^{-\lambda M}} \right)}{\lambda M}. \qquad (9)$$

This correction for the time of the measurement was necessary, especially in cases where the measuring time was in the range of the nuclide half-life (t$_R$ > 0.1 t$_{1/2}$). In cases where a multidecay analysis was desired, α was set as 0.5 as soon as the measuring time t$_R$ exceeded the half-life of the expected shortest-lived nuclide.

Besides metallic monitor and backing foils, liquid samples of mean volumes 1.5 mL were used for counting in cylindrical glass vials (dimensions r$_i$ = 12.8 mm and h = 43 mm). There seemed thus the neccessity of introducing a geometric factor, GF, into formula (8). However, the total GF was in the range of 0.98 for any γ-energy, a sample distance of d = 10 cm and a maximum sample volume of 2 mL. In view of the high particle flux error, a GF correction was neglected.

The determination of separation time t[#] and separation efficiencies (1-κ) and (1-τ) was done carefully. The washing of the precipitate with dilute NaOH was chosen as the separation time. The chromium fraction κ in the Mn-fraction was given by its relative ⁴⁸V content, since vanadium behaves chemically similar to chromium under the chosen separation conditions (cf. above). Below the reaction energy, i.e. practically below deuteron energies of 6 MeV, however, the detection limit for ⁴⁸V in the Mn-fraction was reached and mean experimental data were chosen. For 9 irradiated samples the mean contamination fraction with Cr or V in the Mn-fraction was found to be κ = 0.5 $\pm$ 0.3 %.

The fraction τ of manganese in the Cr-fraction after separation could be quantified principally by using ⁵²Mn, which is formed via the ⁵²Cr(d,2n)⁵²Mn reaction. However, since the threshold of this nuclear reaction is at 8.02 MeV, the nuclide was not formed in many foils. Furthermore, the target nuclide ⁵²Cr was present in the ⁵⁰Cr targets with a relative abundance of only 4.8 %. In those cases, the annihilation radiation − mainly due to ⁵¹Mn − was used to quantify τ. For this purpose the contribution of ⁴⁸V was subtracted from the peak area of the 511 keV γ-line in the Cr-fraction.

Calculation of cross sections

The cross sections for nuclear reactions induced in chromium at various effective projectile energies were calculated using the re-arranged activation formula. As particle flux the calculated weighted mean value inside the stack was used.

Error estimation

The error ΔE_{foil} in the projectile energy effective in each foil of the stack, depending on the incident particle energy ΔE_0, was estimated by using the expression (10) for both deuteron and proton experiments. Incident particle energy error was 0.2 MeV for 14 MeV deuterons as well as for 22 and 40 MeV protons.

$$\Delta E_{foil} = \Delta E_0 \cdot \left(\frac{E_0}{E_{foil}}\right)^{0.76}. \tag{10}$$

Errors of individual fluxes were estimated from the errors of the parameters (activity (A), cross section (σ) and number of target nuclei per plane ($\tilde{N}$)) using the Gaussian error propagation law. While in proton experiments the errors of the final mean fluxes I_x in the stack were calculated as a weighted mean of the individual flux errors, the errors of the final deuteron fluxes were adopted as 16% due to the higher estimated systematic errors in monitor cross sections.

In the case of simple photopeak integration an error belonging to the peak counts I, given by the Gamma-Vision software, takes into account the statistical error as well as the integration error due to high background noise. The error of the detector efficiency $\Delta\varepsilon$ was 6%. In the case of radiochemical separations, liquid samples with mean volumes of 1.5 mL were measured, but no geometric correction factor was considered and thus a maximum geometric error contribution of 2% to the activity error was accepted, as described above. Thus the resulting absolute activity error was $\leq 7\%$.

Errors of the calculated cross sections were determined from the errors of the parameters (activity (A), particle flux (I_x), and number of target nuclei per plane ($\tilde{N}$)) using the Gaussian error propagation law. The error of the number of target nuclei per plane ($\Delta\tilde{N}$) was in the range of 12% in deuteron experiments and 10% and 6.5% in proton irradiations at the CV 28 and COSY injector, respectively. This error contains both the radiochemical separation error and the photometric target mass determination error.

Finally, the errors of the calculated cross sections were found to be in the range of 17 to 27%.

Results and discussion

Deuteron induced nuclear reactions

Cross sections

$^{50}Cr(d,n)^{51}Mn$

As described above, ^{51}Mn was quantified by 4 different methods: 1) 511 keV, non-destructive, ND. The other three methods were applied after chemical separation; in each case the manganese fraction was measured: 2) 511 keV, multidecay analysis, MDA; 3) 320 keV, daughter ^{51}Cr, DAU; and 4) 749 keV, characteristic photopeak, CP. The respective cross section results are listed in Table 4 together with the resulting weighted mean value at each energy. The ND and DAU methods gave consistent results, but in the CP method the scatter was rather large, as expected. Furthermore, the CP data lie on the average 9.6% below the mean data. The DAU data with their mean deviation of 1.1% are consistent with the mean cross sections. Quite far from the mean are also the ND and the MDA data with mean deviations of +9.4 and −8.1%, respectively.

The weighted mean cross sections are shown in Fig. 1 together with the data from the literature. There is some disagreement. Cogneau *et al.* [9] found the maximum cross section of 250 mb at 6.0 MeV whereas our maximum amounted to 215 mb at 5.8 MeV. Furthermore, in contrast to the present results, the literature data show an increase above 10 MeV, presumably due to the use of Cr of natural isotopic composition. A few of our own data show more scatter than those in the literature.

$^{50}Cr(d,2n)^{50m}Mn$

Up to now no cross section data exist in the literature for this reaction. The 1.75 min isomeric state of ^{50}Mn [34] was

Table 4. Cross sections for the $^{50}Cr(d,n)^{51}Mn$ reaction. Data were obtained using 4 different methods.

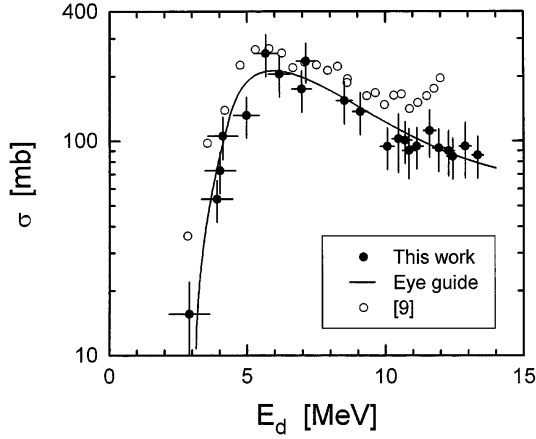| E_d [MeV]	σ ($^{50}Cr(d,n)^{51}Mn$) [mb]				
	511 keV ND (40%)[a]	511 keV MDA (30%)[a]	320 keV DAU (20%)[a]	749 keV CP (10%)[a]	Weighted mean
2.90 ± 0.73	16.5 ± 3.5	12.0 ± 2.5	18.9 ± 19.0	16.2 ± 4.0	15.6 ± 6.3
3.91 ± 0.57	60.1 ± 12.6	47.2 ± 9.9	54.5 ± 13.1	45.6 ± 11.5	53.7 ± 11.8
4.02 ± 0.56	86.1 ± 18.1	61.5 ± 12.9	71.8 ± 17.2	54.7 ± 12.5	72.7 ± 15.8
4.12 ± 0.54	115.6 ± 25.3	98.0 ± 20.5	110.3 ± 27.1	77.8 ± 21.0	105.5 ± 23.4
4.98 ± 0.46	139.9 ± 29.3	119.7 ± 25.0	138.3 ± 32.3	119.3 ± 26.6	131.5 ± 28.4
5.68 ± 0.41		267.4 ± 55.9	196.9 ± 45.8	337.3 ± 79.5	255.6 ± 56.5
6.17 ± 0.39	220.7 ± 46.3	179.7 ± 37.6	208.5 ± 49.0	206.1 ± 48.1	204.5 ± 44.4
6.97 ± 0.35	189.2 ± 39.6	160.0 ± 33.5	181.1 ± 44.0	142.3 ± 31.8	174.1 ± 37.9
7.13 ± 0.34		235.3 ± 49.2			235.3 ± 49.2
8.51 ± 0.29	168.4 ± 35.4	138.5 ± 29.0	168.2 ± 41.4	113.9 ± 31.7	153.9 ± 34.3
9.09 ± 0.28	147.3 ± 31.0	128.0 ± 26.8	140.3 ± 34.0	116.5 ± 30.2	137.0 ± 30.2
10.07 ± 0.25	105.1 ± 22.0	86.2 ± 18.0	96.0 ± 23.5	70.6 ± 16.3	94.2 ± 20.5
10.48 ± 0.25	112.3 ± 23.6	90.9 ± 19.0	105.8 ± 68.0	89.9 ± 21.6	102.3 ± 30.9
10.72 ± 0.24	106.9 ± 22.5	87.8 ± 18.4	108.0 ± 25.6	99.7 ± 25.0	100.7 ± 22.1
10.85 ± 0.24		91.3 ± 19.7		87.5 ± 34.9	90.3 ± 23.5
11.14 ± 0.23	105.8 ± 22.2	85.1 ± 17.8	97.5 ± 23.1	72.2 ± 16.5	94.6 ± 20.5
11.61 ± 0.23		109.5 ± 23.5		117.5 ± 40.3	111.5 ± 27.7
11.94 ± 0.22	103.0 ± 21.7	88.8 ± 18.6	86.6 ± 21.3	75.8 ± 21.1	92.7 ± 20.6
12.29 ± 0.22		83.1 ± 17.4		110.5 ± 33.0	90.0 ± 21.3
12.44 ± 0.21	98.3 ± 20.6	72.7 ± 15.2	86.6 ± 19.9	62.4 ± 14.5	84.7 ± 18.2
12.89 ± 0.21		96.3 ± 20.2		88.5 ± 48.3	94.4 ± 27.2
13.34 ± 0.20	99.5 ± 20.9	75.5 ± 15.8	86.7 ± 20.0	60.8 ± 17.3	85.9 ± 18.8

a: Weighting factor [%]; for details see text.

Fig. 1. Excitation function of the [50]Cr(d,n)[51]Mn reaction. The present data were obtained using enriched [50]Cr and the literature data [9] using [nat]Cr (correcting for the abundance of [50]Cr in [nat]Cr). The solid line is an eye guide.
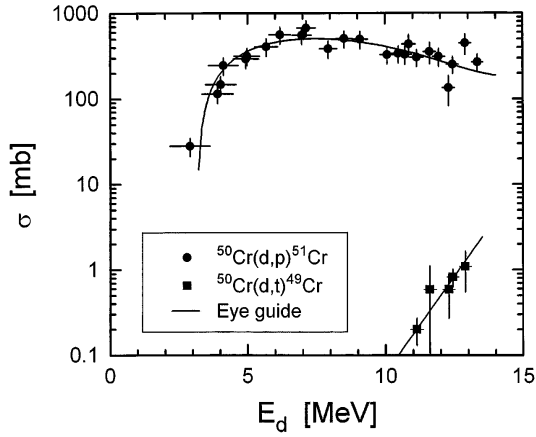

Fig. 2. Excitation function of the nuclear reaction [50]Cr(d,p)[51]Cr, including small contribution from the [52]Cr(d,t)[51]Cr reaction, and of the [50]Cr(d,t)[49]Cr process. Solid lines are eye guides.

Table 5. Cross sections for [50]Cr(d,t)[49]Cr and [52]Cr(d,2p)[52]V reactions.

E_d [MeV]	σ ([50]Cr(d,t)[49]Cr) [mb]	σ ([52]Cr(d,2p)[52]V) [mb]
11.14 ± 0.23	0.20 ± 0.07	
11.61 ± 0.23	0.59 ± 0.51	2.8 ± 2.0
12.29 ± 0.22	0.59 ± 0.32	12.2 ± 3.7
12.44 ± 0.21	0.82 ± 0.19	
12.89 ± 0.21	1.09 ± 0.54	26.5 ± 8.8

observed in this work at our maximum possible effective deuteron energy of 12.89 MeV with a corresponding cross section of 0.87 ± 0.13 mb.

[50]Cr(d,t)[49]Cr and [52]Cr(d,2p)[52]V

The measured data for these reactions are given in Table 5. The results for the [50]Cr(d,t)[49]Cr (calculated threshold: 7.02 MeV) reaction are shown in Fig. 2. Contributions from the [50]Cr(d,d'n)[49]Cr reaction are not relevant for 13 MeV deuterons, since the calculated threshold of 13.53 MeV is too high. In the observed energy range, the cross section increases with the increasing deuteron energy.
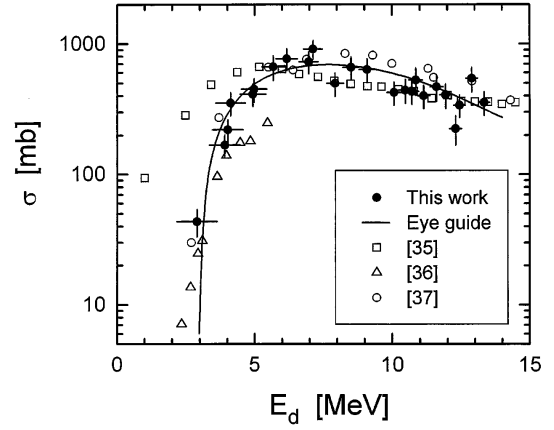

Fig. 3. Cumulative cross sections for the nuclear processes [50]Cr(d,p)[51]Cr + [50]Cr(d,n)[51]Mn → [51]Cr {+ small contribution from [52]Cr(d,t)[51]Cr}. Both present and literature data are included. The solid line is an eye guide.

Table 6. Cumulative cross sections for the formation of ^{51}Cr via {[50]Cr(d,p)[51]Cr + [50]Cr(d,n)[51]Mn → [51]Cr} process and cross sections for the [50]Cr(d,p)[51]Cr and [50]Cr(d,α)[48]V nuclear reactions.

E_d [MeV]	σ [50]Cr(d,x)[51]Cr [mb]		σ [50]Cr(d,α)[48]V [mb]
	(d,p)[a]	[(d,p) + (d,n)][a]	
2.90 ± 0.73	27.9 ± 6.7	43.5 ± 10.3	0.28 ± 0.08
3.91 ± 0.57	114.5 ± 26.1	168.1 ± 32.3	1.75 ± 0.38
4.02 ± 0.56	147.4 ± 34.3	220.1 ± 42.7	2.76 ± 0.61
4.12 ± 0.54	245.7 ± 56.4	351.2 ± 71.0	5.30 ± 1.15
4.94 ± 0.47	294.0 ± 67.8	410.2 ± 80.2	8.41 ± 1.77
4.98 ± 0.46	316.5 ± 71.7	448.0 ± 89.5	7.92 ± 1.68
5.68 ± 0.41	408.8 ± 93.6	664.4 ± 143.3	20.0 ± 4.2
6.17 ± 0.39	562.2 ± 124.8	766.7 ± 147.4	25.42 ± 5.4
6.97 ± 0.35	552.4 ± 121.5	726.5 ± 139.3	30.0 ± 6.3
7.13 ± 0.34	674.7 ± 141.6	910.0 ± 149.9	32.8 ± 6.9
7.94 ± 0.31	386.7 ± 87.9	495.9 ± 100.5	31.6 ± 6.6
8.51 ± 0.29	505.4 ± 112.4	659.3 ± 130.2	52.4 ± 11.1
9.09 ± 0.28	497.9 ± 114.8	634.9 ± 131.2	63.6 ± 13.3
10.07 ± 0.25	328.8 ± 72.6	423.0 ± 84.6	47.2 ± 9.9
10.48 ± 0.25	338.2 ± 75.3	440.5 ± 90.5	56.4 ± 11.9
10.72 ± 0.24	330.4 ± 77.4	431.1 ± 87.7	61.0 ± 12.8
10.85 ± 0.24	435.3 ± 127.2	525.6 ± 124.1	71.6 ± 15.9
11.14 ± 0.23	305.5 ± 67.8	400.0 ± 80.4	59.3 ± 12.4
11.61 ± 0.23	354.8 ± 98.7	466.3 ± 104.8	73.8 ± 15.7
11.94 ± 0.22	312.7 ± 73.8	405.5 ± 85.8	89.0 ± 18.6
12.29 ± 0.22	134.5 ± 51.4	224.5 ± 56.8	55.8 ± 11.9
12.44 ± 0.21	253.4 ± 56.4	338.1 ± 66.0	56.1 ± 11.8
12.89 ± 0.21	448.0 ± 121.0	542.3 ± 116.5	64.9 ± 13.8
13.34 ± 0.20	268.9 ± 62.9	354.7 ± 73.1	59.5 ± 12.5

a: This process contains additionally small contribution from the [52]Cr(d,t)[51]Cr reaction.

[50]Cr(d,p)[51]Cr

Both cumulative and independent formation cross sections of ^{51}Cr are listed in Table 6. The cross sections presented in the literature [35−37] are all cumulative, i.e. a sum of [50]Cr(d,p) and [50]Cr(d,n) reactions, and disagree to some extent, (cf. Fig. 3). The data of Kafalas and Irvine [35] appear to be shifted to lower energies; in particular the reaction threshold is very low. Those authors used chromium of natural isotopic abundance, thus including to some extent the contribution of the [52]Cr(d,t) reaction above 10 MeV.
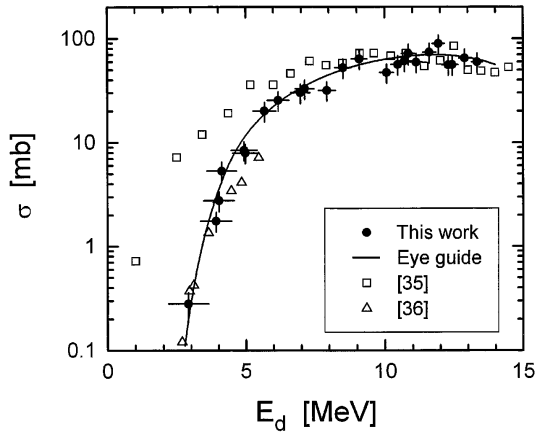
Fig. 4. Excitation function of the ^{50}Cr(d,α)^{48}V reaction. Both present and literature data are included. The solid line is an eye guide.

Fig. 5. Integral yields of the nuclear reactions ^{50}Cr(d,n)^{51}Mn, ^{50}Cr(d,p)^{51}Cr, ^{50}Cr(d,α)^{48}V and ^{50}Cr(d,t)^{49}Cr, calculated from the excitation functions determined in this work.

The cross sections of Coetzee and Preisach [36] show a reaction threshold similar to ours, but their data are about 50% below our values. The cross sections found by Bisconti *et al.* [37], using ^{nat}Cr as target, correspond to some extent to our data. The data for the pure ^{50}Cr(d,p)^{51}Cr reaction, obtained after various corrections, are reported for the first time and are shown in Fig. 2. Evidently it is a much stronger reaction channel than the (d,n) reaction shown in Fig. 1.

^{50}Cr(d,α)^{48}V

Cross sections for this reaction are given in Table 6 and Fig. 4, together with the literature data. The behaviour of the data of Kafalas and Irvine [35] and Coetzee and Preisach [36] is similar to that for the ^{50}Cr(d,p) reaction. In particular the data of Kafalas and Irvine [35] near the threshold appear to be wrong. Our reaction threshold is at about 3 MeV and the maximum of the excitation function at 11.5 MeV amounts to 72 mb.

Table 7. Cross sections for the nuclear process ^{nat}Cr(p,x)^{51}Mn. Data were obtained using 2 different determination methods.

E_p [MeV]	σ (^{nat}Cr(p,x)^{51}Mn) [mb]		
	511 keV MDA (75%)[a]	749 keV CP (25%)[a]	Weighted mean
17.39 ± 0.48	13.8 ± 3.9	19.2 ± 8.2	15.2 ± 5.0
18.47 ± 0.46	38.7 ± 10.8	45.5 ± 14.9	40.4 ± 11.9
19.08 ± 0.22	38.8 ± 7.2	38.7 ± 10.0	38.8 ± 7.9
19.74 ± 0.22	49.3 ± 9.0	48.3 ± 11.5	49.0 ± 9.6
20.06 ± 0.38	46.1 ± 6.1	70.0 ± 16.7	52.0 ± 8.7
20.22 ± 0.21	55.5 ± 8.3	58.3 ± 11.8	56.2 ± 9.2
20.84 ± 0.21	62.0 ± 9.0	65.2 ± 12.9	62.8 ± 10.0
22.72 ± 0.34	68.4 ± 9.1	91.1 ± 19.0	74.1 ± 11.6
25.15 ± 0.32	72.1 ± 9.5	94.3 ± 19.6	77.6 ± 12.0
27.42 ± 0.30	71.6 ± 9.4	57.8 ± 11.4	68.2 ± 9.9
29.55 ± 0.28	58.5 ± 7.8	53.5 ± 10.9	57.3 ± 8.6
31.57 ± 0.27	42.4 ± 5.7	36.5 ± 8.3	40.9 ± 6.3
33.49 ± 0.25	34.6 ± 4.6	38.6 ± 11.0	35.6 ± 6.2
35.67 ± 0.24	26.8 ± 3.6	27.1 ± 9.9	26.9 ± 5.2
38.08 ± 0.23	24.3 ± 3.2	16.8 ± 6.8	22.5 ± 4.1

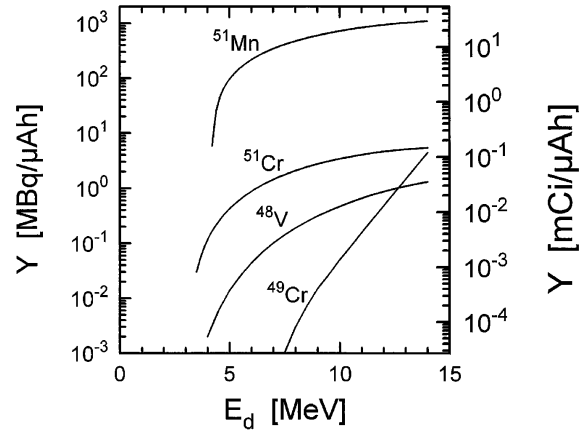a: Weighting factor [%]; for details see text.

Theoretical thick target yields

From the measured excitation functions (see above) the integral yields of the product isotopes were calculated using the well-known integration formula (cf. [38]). In all the calculations an irradiation time of 1 h and a beam current of 1 µA were assumed. The calculated integral yields for deuteron induced reactions on ^{50}Cr are presented in Fig. 5. The ^{50}Cr(d,n) reaction is very promising, since 14 MeV deuterons should give a ^{51}Mn yield of 1.1 GBq/µAh. Most of the non-isotopic nuclides are not important since they can be removed radiochemically. Only ^{52m}Mn might contribute to some extent (below 5%) to the total positron emission, depending on the degree of enrichment of ^{50}Cr ($\geq$ 95%) and the upper energy limit on the target.

Proton induced nuclear reactions

Cross sections

^{nat}Cr(p,x)^{51}Mn

This nuclear reaction was of special interest, since it was not clear, whether this reaction, starting from ^{nat}Cr, could serve as an alternative production route for ^{51}Mn, compared to the ^{50}Cr(d,n) reaction. Cross sections for the formation

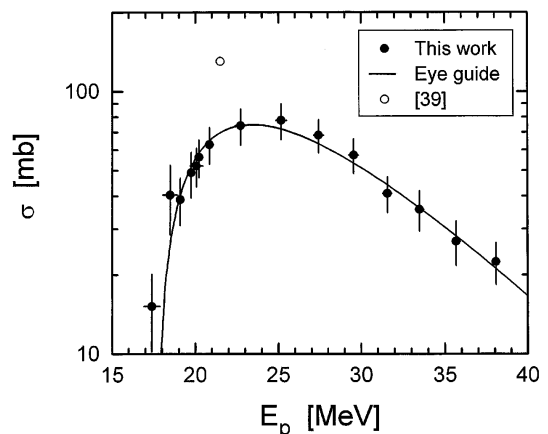**Fig. 6.** Excitation function of the nuclear reaction ^{nat}Cr(p,x)^{51}Mn. The solid line is an eye guide.

Table 8. Cross sections for the nuclear reactions ^{nat}Cr(p,x)^{54}Mn, ^{nat}Cr(p,x)^{52g*}Mn and ^{nat}Cr(p,x)^{52m}Mn and isomeric cross section ratios for the nuclear isomeric pair ^{52m,g}Mn.

E_p [MeV]	σ (^{nat}Cr(p,x)) [mb]			^{52}Mn isomeric cross section ratio σ_m/σ_{g*}
	^{54}Mn	^{52g*}Mn	^{52m}Mn	
17.39 ± 0.48	2.48 ± 0.73	51.7 ± 14.8	–	–
18.47 ± 0.46	2.04 ± 0.60	43.6 ± 12.5	–	–
19.08 ± 0.22	2.99 ± 0.70	$50.0 \pm\ \ 9.7$	69.9 ± 13.6	1.40 ± 0.14
19.74 ± 0.22	1.90 ± 0.46	$42.1 \pm\ \ 8.0$	58.8 ± 11.2	1.40 ± 0.13
20.06 ± 0.38	2.05 ± 0.33	$48.6 \pm\ \ 7.1$	$63.0 \pm\ \ 9.3$	1.30 ± 0.10
20.22 ± 0.21	1.72 ± 0.28	$39.1 \pm\ \ 6.2$	$46.9 \pm\ \ 7.5$	1.20 ± 0.10
20.84 ± 0.21	1.87 ± 0.34	$36.0 \pm\ \ 5.7$	$52.8 \pm\ \ 8.4$	1.47 ± 0.12
22.72 ± 0.34	1.23 ± 0.20	$30.3 \pm\ \ 4.4$	$38.7 \pm\ \ 5.7$	1.28 ± 0.10
25.15 ± 0.32	1.00 ± 0.17	$23.6 \pm\ \ 3.4$	$29.8 \pm\ \ 4.5$	1.26 ± 0.09
27.42 ± 0.30	1.04 ± 0.17	$20.2 \pm\ \ 2.9$	$25.6 \pm\ \ 3.8$	1.27 ± 0.09
29.55 ± 0.28	0.92 ± 0.16	$16.9 \pm\ \ 2.5$	$22.3 \pm\ \ 3.4$	1.32 ± 0.10
31.57 ± 0.27	0.81 ± 0.14	$13.3 \pm\ \ 2.0$	$18.2 \pm\ \ 2.7$	1.37 ± 0.10
33.49 ± 0.25	0.76 ± 0.13	$12.2 \pm\ \ 1.8$	$17.9 \pm\ \ 2.7$	1.47 ± 0.11
35.67 ± 0.24	0.66 ± 0.12	$10.4 \pm\ \ 1.5$	$16.0 \pm\ \ 2.4$	1.54 ± 0.12
38.08 ± 0.23	0.68 ± 0.13	$9.2 \pm\ \ 1.4$	$14.7 \pm\ \ 2.2$	1.59 ± 0.12

^{52g*}Mn denotes cumulative value (see text).

of ^{51}Mn were determined both via the MDA (511 keV, multidecay analysis) and the CP method (749 keV, characteristic photopeak). Individual cross sections as well as the weighted mean values are listed in Table 7. Based on the chosen weighting, the CP data show more scatter than the MDA data, as expected. The mean cross sections are shown in Fig. 6, together with an early value by Cohen and Newman [39], which appears to be in error due to the use of a GM counter. The resulting experimental excitation function, constituted mainly by the ^{52}Cr(p,2n)^{51}Mn reaction, has a threshold at 17.8 MeV; the maximum cross section of 75 mb occurs at about 23 MeV.

^{nat}Cr(p,x)^{52m,g}Mn

^{52g}Mn is formed independently via nuclear processes and partly via the decay of the isomeric state ^{52m}Mn, thus resulting in cumulative ^{52g*}Mn. The independent and cumulative yields, however, differ only slightly, since the metastable state decays only 1.75% by isomeric transition [1]. In Table 8 the cross sections for the formation of both the isomers are given and Fig. 7 shows the present cross sections together with the more reliable data from the literature
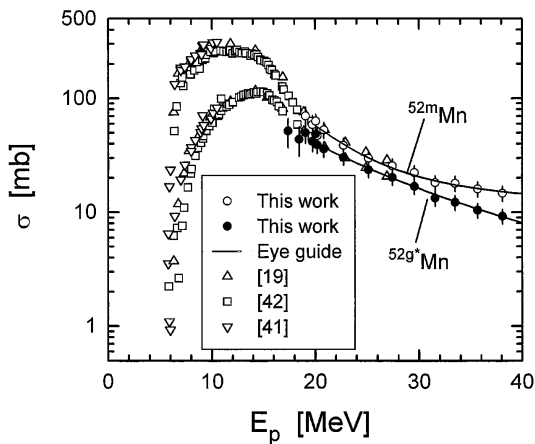
[19, 40−42]. Further data are available for the threshold area [43−46], the high energy region above 100 MeV [47−51] as well as for the sum of the two processes ($^{52m+g}$Mn) [52]. The formation of ^{52m,g}Mn is dominated by the ^{52}Cr(p,n) process. Our data extend the presently known excitation function to medium energies up to 40 MeV.

It is interesting to plot the isomeric cross section ratio as a function of proton energy (cf. Fig. 8 and Table 8). There is a dramatic decrease between 9 and 20 MeV. It is understandable in terms of the spins of the two isomers. The metastable state with a spin of 2^+ is favourably formed at low projectile energies. With increasing energy the higher spin ground state (6^+) is more favourably formed and thus the ratio decreases. The slight increase in the ratio beyond 22 MeV may be due to some contributions from higher energy ^{53}Cr(p,2n)- and ^{54}Cr(p,3n)-processes which tend to favour the higher spin isomer (cf. [53]).

^{nat}Cr(p,x)^{54}Mn

The measured cross sections are listed in Table 8 and shown in Fig. 9. The formation of ^{54}Mn is dominated by

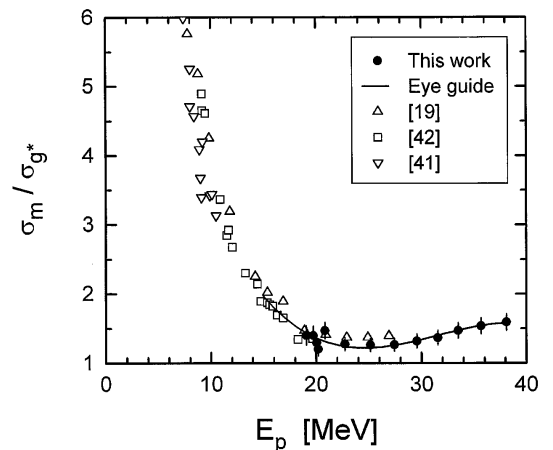**Fig. 7.** Excitation functions of the nuclear reactions ^{nat}Cr(p,x)^{52g*}Mn and ^{nat}Cr(p,x)^{52m}Mn. The solid lines give eye guides.

Fig. 8. Isomeric cross section ratio $\sigma(^{52m}$Mn)$/\sigma(^{52g*}$Mn) for the reaction ^{nat}Cr(p,x)^{52m,g}Mn as a function of projectile energy. The solid line is an eye guide.

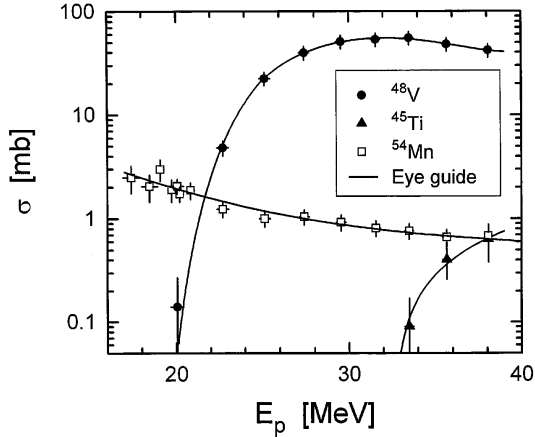**Fig. 9.** Excitation functions of the nuclear reactions $^{nat}Cr(p,x)^{48}V$, $^{nat}Cr(p,x)^{45}Ti$ and $^{nat}Cr(p,x)^{54}Mn$. The solid lines are eye guides.

Fig. 10. Excitation functions of the nuclear reactions $^{nat}Cr(p,x)^{48}Cr$, $^{nat}Cr(p,x)^{49}Cr$ and $^{nat}Cr(p,x)^{51}Cr$. The data for ^{51}Cr describe independent formation cross sections. The solid lines give eye guides.

the $^{54}Cr(p,n)^{54}Mn$ reaction, since the contribution of the $^{53}Cr(p,\gamma)^{54}Mn$ reaction is expected to be negligibly low, especially at the incident energies above 17 MeV. The overall cross section values are, however, low since the abundance of ^{54}Cr in ^{nat}Cr is only 2.365%. Some data were reported previously in the threshold region between 2.2 and 5.5 MeV [54] as well as at higher energies of 370 and 600 MeV [49] and [51]. Our data describe the first study in the region between 18 and 40 MeV.

$^{nat}Cr(p,x)^{48,49}Cr$

The measured cross sections of the $^{nat}Cr(p,x)^{48}Cr$ and $^{nat}Cr(p,x)^{49}Cr$ reactions are listed in Table 9 and shown in Fig. 10. The main contributing processes to the formation of ^{48}Cr are $^{50}Cr(p,t)$ and $^{50}Cr(p,p2n)$. Since the experimental reaction threshold lies above 26 MeV, the contribution of the (p,t) reaction (threshold 15.4 MeV) is obviously small compared to that of the (p,p2n) reaction (threshold 24.1 MeV). Cross sections of proton induced nuclear reactions on chromium leading to ^{48}Cr formation are available at 370 and 600 MeV [51, 55]. Our results describe first studies below 100 MeV.

The major contributing reaction in the case of the $^{nat}Cr(p,x)^{49}Cr$ process is the $^{50}Cr(p,pn)$ reaction with a threshold of 13.26 MeV. No data exist in the literature, except for 370 MeV protons [48].

$^{nat}Cr(p,x)^{51}Cr$

^{51}Cr is mainly formed by the $^{52}Cr(p,pn)^{51}Cr$ reaction, but also by ^{51}Mn decay after $^{52}Cr(p,2n)^{51}Mn$ reaction. Both the measured cumulative and derived independent cross sections are listed in Table 9. The reduced cross sections for the direct $^{nat}Cr(p,x)^{51}Cr$ process, shown in Fig. 10, are on average $11.4 \pm 2.4\%$ lower than the cumulative data. The maximum cross section 523 mb occurs at about 25 MeV. The available knowledge on such independent cross sections in the literature [39] is generally poor compared to that on the cumulative data. The cumulative cross sections are shown in Fig. 11 together with the literature data [42, 56]. The transition from the low energy region to the higher energy range is good. Single data points also exist in the energy range above 100 MeV [49, 51]. In general, however, despite the long half-life of the nuclide, the available knowledge on this nuclear process is limited.

Table 9. Cross sections for the nuclear reactions $^{nat}Cr(p,x)^{48}Cr$, $^{nat}Cr(p,x)^{49}Cr$, $^{nat}Cr(p,x)^{51}Cr$ and cumulative cross sections for the processes $\{^{nat}Cr(p,x)^{51}Cr + ^{nat}Cr(p,x)^{51}Mn \rightarrow ^{51}Cr\}$.

E_p [MeV]	σ ($^{nat}Cr(p,x)$) [mb]			
	^{48}Cr	^{49}Cr	^{51}Cr	$^{51}Cr_{cumulative}$
17.39 ± 0.48		4.29 ± 1.24	242 ± 73	255 ± 76
18.47 ± 0.46		6.92 ± 1.99	304 ± 92	342 ± 102
19.08 ± 0.22		6.18 ± 1.21	402 ± 113	441 ± 118
19.74 ± 0.22		7.27 ± 1.40	377 ± 97	426 ± 104
20.06 ± 0.38		6.62 ± 0.99	444 ± 67	490 ± 72
20.22 ± 0.21		7.31 ± 1.17	411 ± 81	466 ± 87
20.84 ± 0.21		8.51 ± 1.36	433 ± 89	495 ± 95
22.72 ± 0.34		9.43 ± 1.41	485 ± 73	554 ± 81
25.15 ± 0.32		10.60 ± 1.58	499 ± 75	571 ± 84
27.42 ± 0.30	0.08 ± 0.03	11.61 ± 1.69	511 ± 79	583 ± 87
29.55 ± 0.28	0.16 ± 0.03	11.52 ± 1.72	493 ± 75	552 ± 82
31.57 ± 0.27	0.34 ± 0.05	9.44 ± 1.40	409 ± 63	452 ± 68
33.49 ± 0.25	0.58 ± 0.09	8.14 ± 1.31	352 ± 54	387 ± 58
35.67 ± 0.24	0.85 ± 0.15	7.02 ± 1.11	288 ± 44	315 ± 47
38.08 ± 0.23	1.15 ± 0.18	6.15 ± 0.94	261 ± 40	285 ± 42

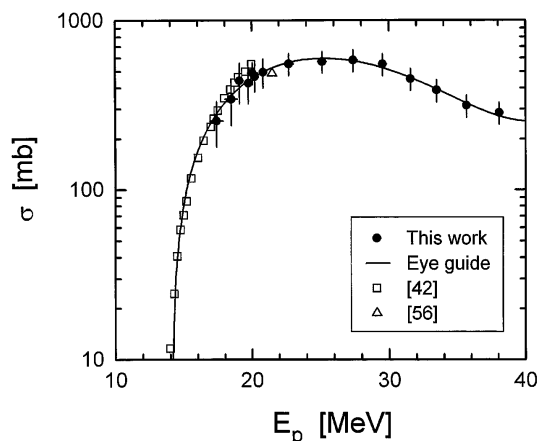**Fig. 11.** Cumulative cross sections for the formation of ^{51}Cr via proton induced nuclear reactions on ^{nat}Cr. The data include contributions of the ^{51}Mn decay. The solid line is an eye guide.

Table 10. Cross sections for the nuclear processes ^{nat}Cr(p,x)^{48}V and ^{nat}Cr(p,x)^{45}Ti.

E_p [MeV]	σ (^{nat}Cr(p,x)) [mb]	
	^{48}V	^{45}Ti
17.39 ± 0.48		
18.47 ± 0.46		
19.08 ± 0.22		
19.74 ± 0.22		
20.06 ± 0.38	0.14 ± 0.14	
20.22 ± 0.21		
20.84 ± 0.21		
22.72 ± 0.34	4.83 ± 0.79	
25.15 ± 0.32	22.4 ± 3.3	
27.42 ± 0.30	39.6 ± 6.0	
29.55 ± 0.28	50.7 ± 7.6	
31.57 ± 0.27	53.5 ± 8.0	
33.49 ± 0.25	55.1 ± 8.2	(0.09 ± 0.09)
35.67 ± 0.24	47.9 ± 7.2	0.40 ± 0.14
38.08 ± 0.23	41.9 ± 6.2	0.63 ± 0.25

^{nat}Cr(p,x)^{48}V and ^{nat}Cr(p,x)^{45}Ti

The measured cross sections for these two processes are listed in Table 10 and shown graphically in Fig. 9. ^{48}V is formed mainly via the ^{52}Cr(p,αn)^{48}V reaction (threshold 14.42 MeV). The maximum cross section of 55 mb occurs at about 32 MeV. Literature data are nearly unknown except for proton energies of 370 and 600 MeV [51, 55].

^{45}Ti can be induced by ^{50}Cr(p,αpn) reaction (threshold 22.19 MeV). However, the difficulty of its exact determination caused a relatively high uncertainty (cf. above). Literature data are poorly known up to now.

Theoretical thick target yields

The integral yields of radioisotopes produced in the proton induced reactions on ^{nat}Cr were calculated from the excitation functions given above. The results are plotted in Figs. 12 and 13 as a function of incident proton energy. The desired positron emitter ^{51}Mn is accompanied by high activities of radioactive isotopes, especially the short-lived ^{52m}Mn. There is no energy window which could improve
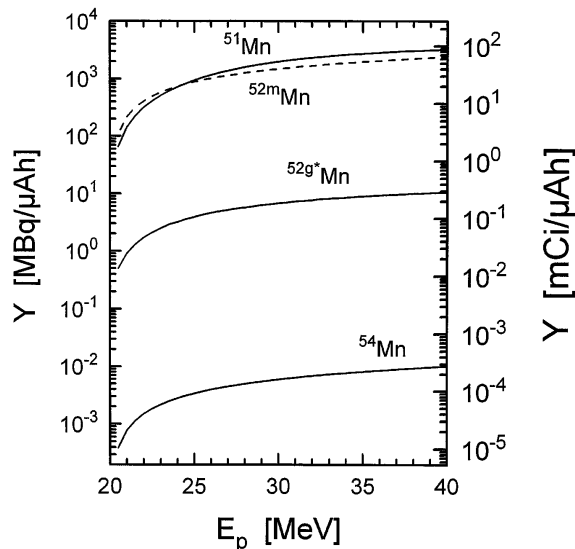

Fig. 12. Integral yields of the radioisotopes ^{51}Mn, ^{52m}Mn, ^{52g*}Mn and ^{54}Mn formed by ^{nat}Cr(p,x) nuclear reactions.
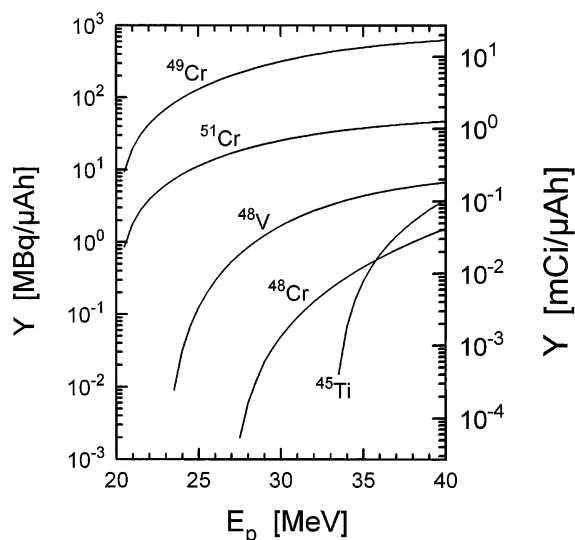

Fig. 13. Integral yields of the radionuclides ^{48}Cr, ^{49}Cr, ^{51}Cr, ^{48}V and ^{45}Ti formed by ^{nat}Cr(p,x) nuclear reactions.

the activity ratio A(^{51}Mn)/A(^{52m}Mn) at EOB. However, the ratio becomes better during the cooling time after EOB, e.g. during chemical separation and labelling procedures. Thus, the activity fraction of ^{51}Mn relative to the sum of all occurring radioisotopes of manganese rises from initially about 60% to about 80% at 1 h after EOB. Simultaneously however, the initial absolute ^{51}Mn activity decays down to about 40%.

Comparison of ^{50}Cr(d,n)^{51}Mn and ^{52}Cr(p,2n)^{51}Mn reactions with respect to the production of ^{51}Mn

In view of the desired PET application, radioisotopically pure ^{51}Mn can in principle be produced only using the ^{50}Cr(d,n) reaction. In the case of ^{52}Cr(p,2n)^{51}Mn reaction, especially while using ^{nat}Cr as target material, the chemi-

cally separated radiomanganese fraction contains ^{52m}Mn and ^{52}Mn in appreciable activities in addition to ^{51}Mn. Only ^{54}Mn can be avoided, if highly enriched ^{52}Cr is used as target.

The yield of ^{51}Mn for $E_p = 40 \rightarrow 20$ MeV using ^{nat}Cr as target material amounts to 3.2 GBq/µAh and is higher than the yield of 1.1 GBq/µAh in the case of the ^{50}Cr(d,n)^{51}Mn reaction at $E_d = 14 \rightarrow 3$ MeV. The required respective target chromium layers are 1600 and 200 mg/cm^2. Thus the ^{nat}Cr(p,x) process demands an 8-fold thicker chromium layer than the ^{50}Cr(d,n) reaction, causing problems in target preparation as well as in the separation process, since about 2 g of compact chromium would only slowly be leached in hot hydrochloric acid and a quantitative separation of target chromium from radiomanganese would hardly be realized. Furthermore, a larger-sized cyclotron is needed to apply the ^{52}Cr(p,2n) reaction, compared to the ^{50}Cr(d,n) route.

In conclusion, the ^{50}Cr(d,n)^{51}Mn reaction is the most promising nuclear process for the production of the positron emitter ^{51}Mn, because firstly, a small cyclotron is sufficient to obtain good ^{51}Mn yields, secondly radioisotopically pure ^{51}Mn is producible, thirdly relatively thin metal layers of target chromium are sufficient for production runs, and fourthly all other radionuclides, especially the positron emitter ^{49}Cr, formed in "side reactions", can be quantitatively chemically separated from the desired ^{51}Mn in one step [33]. However, highly enriched ^{50}Cr as target chromium is needed, but it can be recycled with high efficiency, as already established [12].

References

1. Browne, E., Firestone, R. B.: *Table of Radioactive Isotopes*, V. S. Shirley (Ed.), John Wiley & Sons, New York, USA (1986).
2. Lieser, K. H.: *Einführung in die Kernchemie*, VCH Publishers, Weinheim, Germany (1991).
3. Lambrecht, R. M., Wolf, A. P.: J. Labelled Cpd. Radiopharm. **16**, 129 (1979).
4. Hichwa, R. D., Nickles, R. J.: IEEE Trans. Nucl. Sci. **NS-28**, 1924 (1981).
5. Hichwa, R. D., Daube, M. E., Nickles, R. J.: J. Labelled Cpd. Radiopharm. **18**, 227 (1981).
6. Harper, P. V., Lathrop, K. A., Ryan, J. W.: *Quantitative Studies in Radiopharmaceutical Science, Manganese-51 for Myocardial Localization*, in: R. N. Beck, M. D. Cooper (Eds.), *Nuclear Medicine and Imaging Research*, Progress Report DOE/EV/10359−3, January 1 (1980)−December 31 (1982), The Franklin McLean Memorial Research Institute, University of Chicago, USA (1982).
7. Harper, P. V., Lathrop, K. A., Ryan, J. W.: *Quantitative Studies in Radiopharmaceutical Science*, A.2 *Production of Manganese-51*, in: R. N. Beck, M. D. Cooper (Eds.), Nuclear Medicine and Imaging Research, Progress Report DOE/EV/10359−4, January 1−December 31, The Franklin McLean Memorial Research Institute, University of Chicago, USA (1983).
8. Daube, M. E., Nickles, R. J.: Int. J. Nucl. Med. Biol. **12**, 303 (1985).
9. Cogneau, M., Gilly, L., Cara, J.: Nucl. Phys. **79**, 203 (1966).
10. Mushtaq, A., Qaim, S. M.: Radiochim. Acta **50**, 27 (1990).
11. Fessler, A., Alfassi, Z. B., Qaim, S. M.: Radiochim. Acta **65**, 207 (1994).
12. Klein, A. T. J., Rösch, F., Qaim, S. M.: J. Electrochem. Soc. **146**, 4526 (1999).
13. Blessing, G., Bräutigam, W., Böge, H. G., Gad, N., Scholten, B., Qaim, S. M.: Appl. Radiat. Isot. **46**, 955 (1995).
14. Weinreich, R., Schult, O., Stöcklin, G.: Int. J. Appl. Radiat. Isot. **25**, 535 (1974).
15. Qaim, S. M., Stöcklin, G., Weinreich, R.: Int. J. Appl. Radiat. Isot. **28**, 947 (1977).
16. Piel, H., Qaim, S. M., Stöcklin, G.: Radiochim. Acta **57**, 1 (1992).
17. Williamson, C. F., Boujot, J.-P., Picard, J.: *Tables of Range and Stopping Power of Chemical Elements for Charged Particles of Energy 0.05 to 500 MeV*, Rapport CEA-R 3042, July (1966).
18. Vlasov, N. A. Kalinin, S. P., Oglobin, A. A., Pankramov, V. M., Rudakov, V. P., Serikov, I. N., Sidorov, V. A.: Soviet J. Atomic Energy **2**, 189 (1957).
19. West, H. I. Jr., Lanier, R. G., Mustafa, M. G.: Phys. Rev. C **35**, 2067 (1987).
20. Vandenbosch, R., Huizenga, J. R.: Phys. Rev. **120**, 1313 (1960).
21. Chen, K. L., Miller, J. M.: Phys. Rev. **134**, B1269 (1964).
22. Zaman, M. R., Qaim, S. M.: Radiochim. Acta **75**, 59 (1996).
23. Takács, S., Sonck, M., Scholten, B., Hermanne, A., Tárkányi, F.: Appl. Radiat. Isot. **48**, 657 (1997).
24. Kopecký, P.: Int. J. Appl. Radiat. Isot. **36**, 657 (1985).
25. Mills, S. J., Steyn, G. F., Nortier, F. M.: Appl. Radiat. Isot. **43**, 1019 (1992).
26. Collé, R., Kishore, R., Cumming, J. B.: Phys. Rev. **C9**, 1819 (1974).
27. Lagunas-Solar, M. C., Carvacho, O. F., Cima, R. R.: Appl. Radiat. Isot. **39**, 41 (1988).
28. Furukawa, M., Kume, S., Ogawa, M.: Nucl. Phys. **69**, 362 (1965).
29. Schwerer, O., Okamoto, K.: *Status Report on Cross-Sections of Monitor Reactions for Radioisotope Production*, Report INC(NDS)-218/GZ+, IAEA Nuclear Data Section, Vienna, Austria (1989).
30. Kormány, Z.: Nucl. Instr. Meth. **A337**, 258 (1994).
31. Scholten, B., Qaim, S. M., Stöcklin, G.: Radiochim. Acta **65**, 81 (1994).
32. Fessler, A., Qaim, S. M.: Radiochim. Acta **72**, 121 (1996).
33. Klein, A. T. J.: *Produktion von n.c.a. ^{51}Mn zur in vivo PET-Evaluierung von Kontrastmitteln für die Magnetresonanztomographie (MRT)*, Ph.D. Dissertation, Universität zu Köln, Germany (1997), and report of the Forschungszentrum Jülich, Jül-3553, Germany (1998).
34. Sutton, D. C.: *Half-lives of and isomerism in ^{46}V, ^{50}Mn, ^{54}Co and ^{58}Cu*, Ph.D. Thesis, Nuclear Physics, Princeton University, Princeton, USA (1962).
35. Kafalas, P., Irvine, J. W. Jr.: Phys. Rev. **104**, 703 (1956).
36. Coetzee, P. P., Preisach, M.: Radiochim. Acta **17**, 1 (1972).
37. Bisconti, R., Casteleyn, K., Castiglioni, M., Fossati, F., Manes, L., Stroosnijder, M. F.: Nucl. Instr. Meth. Phys. Res. **B88**, 282 (1994).
38. Qaim, S. M.: Radiochim. Acta **30**, 147 (1982).
39. Cohen, B. L., Newman, E.: Phys. Rev. **99**, 718 (1955).
40. Boehm, F., Marmier, P., Preiswerk, P.: Helv. Phys. Acta **25**, 599 (1952).
41. Wing, J., Huizenga, J. R.: Phys. Rev. **128**, 280 (1962).
42. Barrandon, J. N., Debrun, J. L., Kohn, A., Spear, R. H.: Nucl. Instr. Meth. **127**, 269 (1975).
43. Hemmendinger, A.: Phys. Rev. **58**, 929 (1940).
44. Linder, B., James, R. A.: Phys. Rev. **114**, 322 (1959).
45. Blosser, H. G., Handley, T. H.: Phys. Rev. **100**, 1340 (1955).
46. Taketani, H., Parker, W.: Phys. Rev. **125**, 291 (1962).
47. Valentin, L.: Nucl. Phys. **62**, 81 (1965).
48. Remsberg, L. P., Miller, J. M.: Phys. Rev. **130**, 2069 (1963).
49. Read, J. B. J., Miller, J. M.: Phys. Rev. **B140**, 623 (1965).
50. Reuland, D. J., Caretto, A. A. Jr.: J. Inorg. Nucl. Chem. **31**, 1915 (1969).
51. Michel, R., Dittrich, B., Herpers, U., Pfeiffer, F., Schiffmann, T., Cloth, P., Dragowitsch, P., Filges, D.: Analyst **114**, 295 (1989).
52. Tanaka, S., Furukawa, M.: J. Phys. Soc. Jap. **14**, 1269 (1959).
53. Qaim, S. M., Mushtaq, A., Uhl, M.: Phys. Rev. **C38**, 645 (1988).
54. Johnson, C. H., Galonsky, A., Inskeep, C. N.: Ann. Progr. Rept. ORNL-2910, p. 25 (1960).
55. Karol, P. L., Miller, J. M.: Phys. Rev. **166**, 1089 (1967).
56. Cohen, B. L., Newman, E.: Phys. Rev. **99**, 723 (1955).